IEEE Access
Multidisciplinary | Rapid Review | Open Access Journal

Received December 30, 2020, accepted January 15, 2021, date of publication February 2, 2021, date of current version February 10, 2021.

Digital Object Identifier 10.1109/ACCESS.2021.3055502

Link Adjustment for Assembly Deviation Control of Extendible Support Structures via Sparse Optimization

DEWEN YU, JUNKANG GUO, (Member, IEEE), TENGFEI WU, JUN HONG, (Member, IEEE), AND QIANGQIANG ZHAO

Key Laboratory of Education Ministry for Modern Design and Rotor-Bearing System, School of Mechanical Engineering, Xi'an Jiaotong University, Xi'an 710049, China

Corresponding author: Junkang Guo (guojunkang@gmail.com)

This work was supported in part by the National Natural Science Foundation of China under Grant 51805419 and Grant 51635010, and in part by the China Postdoctoral Science Foundation under Grant 2018M631147 and Grant 2019T120899.

ABSTRACT The assembly accuracy of the extendible support structure is of importance for the imaging capability of synthetic aperture radar antennas. In general, due to manufacturing imperfections and installation variations, its assembly accuracy will be inevitably degraded. Therefore, controlling the assembly deviation is highly concerned in practice. To meet the accuracy requirement and make "the control" more efficient, this study proposes a novel method to quantitatively conduct dimensional adjustment of links for extendible support structures of synthetic aperture radar antennas. Since the extendible support structure is generally over-constrained in the deployed configuration, the relationship between the assembly deviation and the variation sources is first derived by means of equivalent transformation. Based on the mathematical expression of assembly deviation, an inequality constrained sparse optimization model for quantitatively resizing links is formulated. Then, an efficient algorithm integrating the alternating direction method of multipliers and binary search is developed to solve the above optimization model, thereby acquiring the optimal combination of link adjustment. Finally, numerical case studies are carried out to demonstrate the effectiveness of the proposed method in Matlab, which show that it can not only achieve satisfactory performance in prediction but also significantly improve the assembly efficiency.

INDEX TERMS Assembly deviation, dimensional adjustment, extendible support structure, sparse optimization, structural equivalent transformation, ADMM.

I. INTRODUCTION

With the development of imaging technology, synthetic aperture radar (SAR) antennas have been widely applied in remote sensing [1], [2]. Providing that all the electrical devices function well, the surface accuracy of antennas, to a great extent, determines the work performance of radar [3]. Due to the space limitation of rockets, SAR antennas are folded during the launch and then deployed after entering the predetermined orbit. Here, the extendible support structure (ESS) is designed to support the deployable SAR antennas with a stable and precise configuration [4]. Because of inevitable manufacturing imperfections and installation variations, the ESS often fails to meet the specified accuracy requirement [5]. Therefore, in practical engineering, it is indispensable to conduct dimensional adjustment of support links for achieving satisfactory accuracy. This essential operation naturally gives rise to a question for researchers, that is, how to conduct an accurate link adjustment for the ESS to let the designer get rid of "guessing" the corresponding values repeatedly.

In past decades, investigations on dimensional adjustment of the ESS are scarcely reported. To our knowledge, there are only two references that studied this problem. Specifically, Yang *et al.* [6] defined a complex adjustment amount as the objective function to optimize link adjustment for the multi-loop structure. This method can obtain the adjustment length of each link. However, for the convenience of modeling, they treated the ESS as a planar configuration and removed one of the support links, which results in an obvious discrepancy with the practical spatial structure and therefore

The associate editor coordinating the review of this manuscript and approving it for publication was Hamid Mohammad-Sedighi.

limits the application of their method. Zhao *et al.* [7] developed an enhanced approach of combining the Taguchi method and grey relational analysis to determine the combination of link adjustments. Nevertheless, this work has the same limitation with [6]. Namely, the spatial ESS was simplified as a planar structure. It can be seen that because of excessive simplification, the two works mentioned above, in fact, cannot guide the practical dimensional adjustment of links for the spatial ESS, which just motivates us to conduct this study.

As is known, the goal of resizing links is to find the optimal combination of adjustments to improve the assembly accuracy of the ESS. Therefore, theoretically speaking, the dimensional adjustment of the ESS is actually a constraint combinatorial optimization problem. Mathematically, two questions need to be answered. The one is the relationship between the decision variables and objective function, namely the assembly accuracy analysis. The other is the optimization algorithm that can deal with the assembly constraints and achieve the optimum of assembly accuracy. Answering these questions will face the following challenges. (I) Due to the multiple closed loops in the spatial structure, it is intractable to obtain the theoretical relationship between the variation sources and the assembly deviation. Although the finite element analysis (FEA) is available to calculate shape deformations of the ESS after adjustment, the FEA is time-consuming and only feasible for a given adjustment parameters, which is inapplicable to run tremendous simulations to get the optimal dimension in practical engineering. (II) To avoid the potential reliability degeneration during assembly deviation control, the adjustment length of each link should not exceed the prescribed maximum length. Moreover, in view of the assembly efficiency, it is preferred to adjust fewer links under the same magnitude of deviation reduction. Under these assembly constraints, how to obtain the optimal combination of link adjustment remains to be explored.

Even though studies of dimensional adjustment of the ESS are extremely limited, it is noteworthy that there have been some discussions on accuracy analysis of deployable antennas. For example, Mobrem [8] presented four methods to predict the assembly accuracy of the structure with regard to manufacturing fluctuations, namely Monte Carlo analysis, inverse frequency squared method, direct method and normal mode method. However, all of these methods are based on the FEA, and this indicates that once one of the structural parameters is changed, the model should be performed again to compute the assembly accuracy of the ESS. Although the updating technology [9] is developed to speed up the process of prediction, the FEA is still computationally expensive and time-consuming. As a result, it is more attractive to develop theoretical models rather than simulation analysis [10], [11] for the prediction of assembly accuracy. Yang *et al.* [12] constructed an accuracy analysis model based on the principle of elastic deformation energy. Li *et al.* [13] derived the variation propagation model of the multiple-loop structure and obtained the extreme angular errors of the antenna panels. Recently, Zhao *et al.* [14] provided a novel approach which combined the rotatability laws of kinematic chains [15] with the assembly deviation model of two-link unit. Although the coupling constraints were addressed in [12]–[14], these approaches rely on the planar assumption so that the analysis was not enough to describe the spatial characteristics and assembly deviations of the ESS. In addition, the assembly accuracy analysis approaches proposed for other type extendible structures [16]–[19], such as energy method [20], force density method [21], and dynamic relaxation method [22], are difficult to be transferred into the ESS. On the one hand, compared with cable-net extendible structures, the ESS is of sufficient stiffness, and the key factor affecting the assembly accuracy is the direct geometric deviation rather than the flexible deformation. Thus, these form-finding methods are not suitable for the ESS [17]. On the other hand, due to the existence of installation deviations of joints, the current practice shows that the assembly accuracy may be poor even if the support links of the ESS are under uniform stress. As for the assembly deviation control, it is highlighted that to enable the high assembly efficiency, the support links should be adjusted as few as possible, which indicates the optimization of dimensional adjustment of the ESS is in essence a sparse optimization problem. However, the previous optimization algorithms used in assembly accuracy optimization for deployable structures, including the quadratic programming [23], the advance and retreat algorithm [24], the trust-region method [25] and the Nelder-Mead method [26], are not capable of dealing with the optimization model of dimensional adjustment since they cannot provide sparse solutions.

To remove the limitations of traditional approaches to dimensional adjustment and overcome the deficiency of classical optimization algorithms in tackling sparse problems, this paper aims to develop a novel method of quantitatively resizing support links for the spatial ESS. The mapping relationship from the variation sources to the assembly deviation is first derived by structural equivalent transformation, and then the sparse optimization model of link adjustment considering the assembly efficiency is formulated. By solving this optimization problem, the optimal combination of link adjustment is eventually obtained. The contributions of this study are concluded as follows. (I) Rather than simplifying the ESS to a planar mechanism as adopted in previous works, this study directly constructs the assembly deviation model of the spatial ESS, which is consistent with the practical scenario. (II) To pursue high assembly efficiency, the sparsity is inevitable in the optimization model of dimensional adjustment. Different from previous methods that neglect the potential sparsity, this study takes it into account in formulating the optimization model so as to satisfy the requirement of resizing links as few as possible. (III) A novel efficient algorithm is developed to obtain the adjustment vector by integrating the alternating direction method of multipliers (ADMM) algorithm [27] and the binary search algorithm. In addition to achieving the optimal adjustment on the condition of fixed number of links, the proposed algorithm can also determine

the minimum number of links under the given requirement of assembly deviation control. These contributions not only extend the boundary of accuracy analysis for the ESS from the planar configuration to the spatial configuration but also provide an effective methodology for the deviation control of the ESS, which are beneficial to improve the assembly performance and shorten the assembly cycle.

The remainder of this paper is organized as follows. Section 2 briefly introduces the ESS and develops the assembly deviation model for surface accuracy control. Afterwards, Section 3 proposes the sparse optimization model and the corresponding parameter estimation algorithm. Case studies are provided to verify the performance of the proposed method in Section 4, and the extension of the algorithm is discussed in Section 5. Finally, conclusions are drawn in Section 6.

II. ASSEMBLY DEVIATION MODEL OF THE ESS

A. INTRODUCTION OF THE ESS

As shown in Figure 1, the ESS of the SAR antenna is mainly composed of inner and outer panels, support links and self-locked joints. The 90° self-locked joints are designed to fix the inner panel to the load module, and the 180° self-locked joints are employed to connect the inner panel and the outer panel. For the detailed structure of these self-locked joints, interested readers can get additional information from [4], [13]. Besides, universe rotary joints are adopted in the points A1-A6, O and C. To improve the stiffness and reliability of system, the truss structure, a combination of the outer, middle, inner support links and the auxiliary link, is utilized to support the two antenna panels. In view of the fact, these links are descried as support links for convenience. Remarkably, the ESS is an over-constrained structure with multiple closed loops.

To articulate the problem addressed in this work, one definition is clarified first. The assembly deviation of the ESS refers to the pose error of panels, and it is composed of three small translational displacements and three small rotations expressed in terms of Euler angles. When the length of links and installation positions of joints deviate from their normal values, the assembly deviation of the ESS arises. Therefore, the goal of this study is to find the optimal combination of link adjustments (OA_1, OA_2, OA_3, OA_4, OA_5, OA_6 and OC) to minimize the assembly deviation of the ESS.

B. STRUCTURAL EQUIVALENT TRANSFORMATION

As mentioned above, the ESS is a multiple-closed-loop structure, the equivalent transformation of the structure must be carried out to eliminate the over-constraint. To this end, the ESS is divided into two parts as shown in Figure 2. The first part consists of the antenna panels and the outer, middle and inner links. The second part is composed of the auxiliary link and the virtual link, where the latter represents the first part after assembly.

The reasons for the above transformation are as follows. Due to the fact that the clearance of the 180° self-locked joint

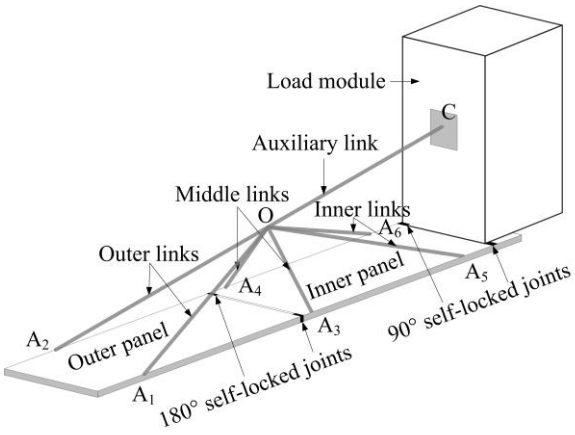

FIGURE 1. ESS of the SAR antenna.

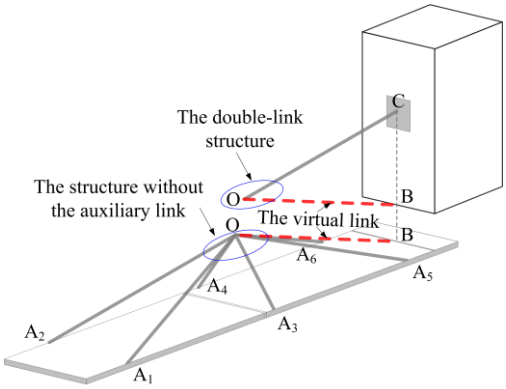

FIGURE 2. Structural equivalent transformation of the ESS.

is small (less than 0.01 mm) and the structural stiffness of the joint is relatively large, the initial deviation of two panels nearly remains constant throughout the whole assembly and adjustment process. Thus, the inner and outer panels can be viewed as a whole plate. Different from the 180° self-locked joints, the 90° joints are designed with larger clearances for reducing the difficulty of assembly, which can tolerate assembly deviation of the panels to a certain extent. In addition, the auxiliary link is not connected to the load module until the first part is completely assembled. As described above, separating the first part from the ESS is consistent with the practice. Once the pose error of panels is determined in the local coordinate system, the virtual link can be utilized to equivalently represent the first part.

In this study, the first part is further regarded as a 6-SPS (S-spherical pair, P-prismatic pair) structure as shown in Figure 3. On the one hand, the dimensional adjustment of links is similar to the linear movement of the prismatic pair because both of them are changing the active length in essence. On the other hand, since all joints exist radial clearances, alternating rotating pairs with spherical pairs is acceptable. As for the second part, it can be simplified into the double-link structure by projection as shown in Figure 4.

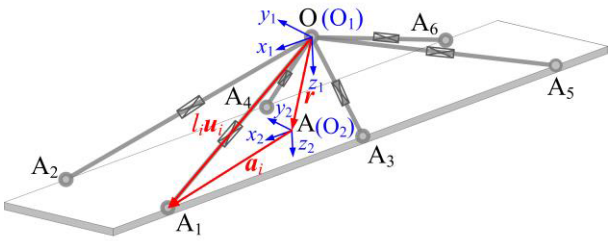

FIGURE 3. Support structure without the auxiliary link.

It is worth mentioning that the rationality of above structural transformation will also be verified by FEA in section 5.1.

C. ASSEMBLY DEVIATION MODELING OF THE STRUCTURE WITHOUT THE AUXILIARY LINK

For quantitative description, a local coordinate system O_1-$x_1y_1z_1$ is established at the intersection center O of the six support links. The x_1 axis is along the length direction of the antenna panel and away from the load module, and the z_1 axis is perpendicular to the panel and points to the panel, and the y_1 axis is determined by the right-hand rule. Besides, another local coordinate system O_2-$x_2y_2z_2$ is established at the geometric center A of the antenna panel, which is parallel to the coordinate system O_1-$x_1y_1z_1$.

For the ith closed loop O-A-A_i-O ($i = 1, 2, 3, 4, 5, 6$), we have

$$l_i\boldsymbol{u}_i = \boldsymbol{r} + \boldsymbol{R}\boldsymbol{a}_i \tag{1}$$

where l_i is the nominal length of the link OA_i; $\boldsymbol{u}_i$ is an unit vector from O to A_i, and $\boldsymbol{r}$ is the vector from O to A in the coordinate system O_1-$x_1y_1z_1$; $\boldsymbol{R}$ is the homogeneous transformation matrix from the coordinate system O_2-$x_2y_2z_2$ to the O_1-$x_1y_1z_1$; $\boldsymbol{a}_i$ is the position coordinates of A_i in the system of O_2-$x_2y_2z_2$.

By taking the derivative of Eq. (1), we get

$$dl_i\boldsymbol{u}_i + l_i d\boldsymbol{u}_i = d\boldsymbol{r} + d\boldsymbol{R}\boldsymbol{a}_i + \boldsymbol{R}d\boldsymbol{a}_i. \tag{2}$$

And then both sides of Eq. (2) are multiplied by $\boldsymbol{u}_i^T$, expressed as

$$\boldsymbol{u}_i^T dl_i\boldsymbol{u}_i + \boldsymbol{u}_i^T l_i d\boldsymbol{u}_i = \boldsymbol{u}_i^T d\boldsymbol{r} + \boldsymbol{u}_i^T d\boldsymbol{R}\boldsymbol{a}_i + \boldsymbol{u}_i^T \boldsymbol{R}d\boldsymbol{a}_i. \tag{3}$$

Due to $d\boldsymbol{R} = \Delta\boldsymbol{R}\boldsymbol{R}$ [28], $\boldsymbol{u}_i^T d\boldsymbol{R}\boldsymbol{a}_i$ can be further derived as

$$\boldsymbol{u}_i^T d\boldsymbol{R}\boldsymbol{a}_i = \boldsymbol{u}_i^T \Delta\boldsymbol{R}\boldsymbol{R}\boldsymbol{a}_i = \boldsymbol{u}_i^T \Delta\theta \times (\boldsymbol{R}\boldsymbol{a}_i) = (\boldsymbol{R}\boldsymbol{a}_i \times \boldsymbol{u}_i)^T \Delta\theta. \tag{4}$$

where $\Delta\boldsymbol{\theta} = [\delta_x, \delta_y, \delta_z]^T$ denotes the orientation deviation of panels in O_1-$x_1y_1z_1$, and $\Delta\boldsymbol{R}$ is defined by

$$\Delta\boldsymbol{R} = \begin{bmatrix} 1 & -\delta_z & \delta_y \\ \delta_z & 1 & -\delta_x \\ -\delta_y & \delta_x & 1 \end{bmatrix} \tag{5}$$

Note that the length deviation is much smaller than the normal length. Hence, the length deviation can be regarded as a small quantity, namely $dl_i = \Delta l_i$, $d\boldsymbol{r} = \Delta\boldsymbol{r}$ and $d\boldsymbol{a}_i = \Delta\boldsymbol{a}_i$. By substituting Eq. (4) into Eq. (2), we obtain

$$\Delta l_i = \boldsymbol{u}_i^T \Delta\boldsymbol{r} + (\boldsymbol{R}\boldsymbol{a}_i \times \boldsymbol{u}_i)^T \Delta\boldsymbol{\theta} + \boldsymbol{u}_i^T \boldsymbol{R}\Delta\boldsymbol{a}_i \tag{6}$$

And Eq. (6) can be expressed in an equivalent form:

$$\Delta l_i = \begin{bmatrix} \boldsymbol{u}_i^T & (\boldsymbol{R}\boldsymbol{a}_i \times \boldsymbol{u}_i)^T \end{bmatrix} \begin{bmatrix} \Delta\boldsymbol{r} & \Delta\boldsymbol{\theta} \end{bmatrix}^T + \begin{bmatrix} \boldsymbol{u}_i^T \boldsymbol{R} \end{bmatrix} [\Delta\boldsymbol{a}_i] \tag{7}$$

where Δl_i represents the deviation of l_i; $\Delta\boldsymbol{r}$ and $\Delta\theta$ denote the position and orientation deviations of panels, respectively.

Since all of the six closed loops satisfy Eq. (2), the compact form of Eq. (7) is expressed by

$$\Delta\boldsymbol{L} = \boldsymbol{J}_v \Delta\boldsymbol{V} + \boldsymbol{J}_b \Delta\boldsymbol{B} \tag{8}$$

where $\Delta\boldsymbol{L} = [\Delta l_1, \Delta l_2, \Delta l_3, \Delta l_4, \Delta l_5, \Delta l_6]^T$; $\Delta\boldsymbol{B} = [\Delta a_1, \Delta a_2, \Delta a_3, \Delta a_4, \Delta a_5, \Delta a_6]^T$ with $\Delta a_i = [\Delta x_i, \Delta y_i, \Delta z_i]$; $\Delta\boldsymbol{V} = [\Delta\boldsymbol{r}, \Delta\theta]^T$; $\boldsymbol{J}_v$ and $\boldsymbol{J}_b$ are the coefficient matrixes, which are defined by

$$\begin{cases} \boldsymbol{J}_v = \begin{bmatrix} \boldsymbol{u}_1^T & (\boldsymbol{R}\boldsymbol{a}_6 \times \boldsymbol{u}_1)^T \\ \boldsymbol{u}_2^T & (\boldsymbol{R}\boldsymbol{a}_6 \times \boldsymbol{u}_2)^T \\ \boldsymbol{u}_3^T & (\boldsymbol{R}\boldsymbol{a}_6 \times \boldsymbol{u}_3)^T \\ \boldsymbol{u}_4^T & (\boldsymbol{R}\boldsymbol{a}_6 \times \boldsymbol{u}_4)^T \\ \boldsymbol{u}_5^T & (\boldsymbol{R}\boldsymbol{a}_6 \times \boldsymbol{u}_5)^T \\ \boldsymbol{u}_6^T & (\boldsymbol{R}\boldsymbol{a}_6 \times \boldsymbol{u}_6)^T \end{bmatrix} \\ \boldsymbol{J}_b = \begin{bmatrix} \boldsymbol{u}_1^T\boldsymbol{R} & \boldsymbol{0} & \boldsymbol{0} & \boldsymbol{0} & \boldsymbol{0} & \boldsymbol{0} \\ \boldsymbol{0} & \boldsymbol{u}_2^T\boldsymbol{R} & \boldsymbol{0} & \boldsymbol{0} & \boldsymbol{0} & \boldsymbol{0} \\ \boldsymbol{0} & \boldsymbol{0} & \boldsymbol{u}_3^T\boldsymbol{R} & \boldsymbol{0} & \boldsymbol{0} & \boldsymbol{0} \\ \boldsymbol{0} & \boldsymbol{0} & \boldsymbol{0} & \boldsymbol{u}_4^T\boldsymbol{R} & \boldsymbol{0} & \boldsymbol{0} \\ \boldsymbol{0} & \boldsymbol{0} & \boldsymbol{0} & \boldsymbol{0} & \boldsymbol{u}_5^T\boldsymbol{R} & \boldsymbol{0} \\ \boldsymbol{0} & \boldsymbol{0} & \boldsymbol{0} & \boldsymbol{0} & \boldsymbol{0} & \boldsymbol{u}_6^T\boldsymbol{R} \end{bmatrix} \end{cases} \tag{9}$$

Thus, utilizing Eq. (8), we can obtain the pose deviation of the first part in O_1-$x_1y_1z_1$:

$$\Delta\boldsymbol{V} = \begin{bmatrix} \boldsymbol{J}_v^{-1} & \boldsymbol{J}_v^{-1}\boldsymbol{J}_b \end{bmatrix} \begin{bmatrix} \Delta\boldsymbol{L} & \Delta\boldsymbol{B} \end{bmatrix}^T. \tag{10}$$

D. ERROR MODELING WITH THE AUXILIARY LINK

After the assembly deviation model of the first part is developed, the auxiliary link is to be considered in this section. As shown in Fig 4, the global coordinate system O_g-$x_gy_gz_g$ is located at the geometric symmetric center of two 90° self-locked joints, which is parallel to the O_1-$x_1y_1z_1$. Note that the pose deviation is definite with respect to the coordinate system O_1-$x_1y_1z_1$ after the first part is assembled. Here, a virtual link is introduced to represent the first part in O_g-$x_gy_gz_g$ for simplicity. It can be observed that both the auxiliary link and the virtual link are in the x_g-z_g plane.

In this case, the position deviation of the point O is calculated by

$$\Delta\boldsymbol{O} = \boldsymbol{\mu}_1\Delta\boldsymbol{l} + \boldsymbol{\mu}_2\Delta\boldsymbol{B} + \boldsymbol{\mu}_3\Delta\boldsymbol{C}. \tag{11}$$

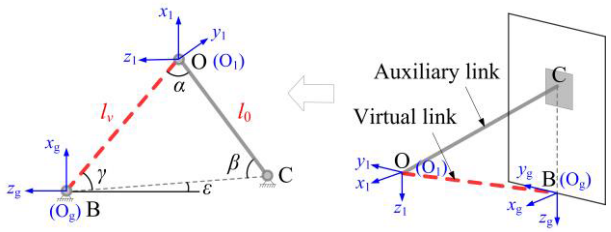

FIGURE 4. Double-link connection structure.

In Eq. (11), $\Delta \boldsymbol{l} = [\Delta l_{\mathrm{v}}, \Delta l_0]^T$, where Δl_{v} and Δl_0 represent the length deviation of the virtual link and the auxiliary link, respectively; $\Delta \boldsymbol{B} = [\Delta z_{\mathrm{B}}, \Delta x_{\mathrm{B}}]^T$, where Δz_{B} and Δx_{B} are the position deviations with respect to z_{g} axis and x_{g} axis, respectively. Similar to $\Delta \boldsymbol{B}$, $\Delta \boldsymbol{C} = [\Delta z_{\mathrm{C}}, \Delta x_{\mathrm{C}}]^T$. Besides, $\boldsymbol{\mu}_1$, $\boldsymbol{\mu}_2$ and $\boldsymbol{\mu}_3$ are the corresponding coefficient matrices, which are derived as

$$\begin{cases} \boldsymbol{\mu}_1 = \begin{bmatrix} \dfrac{\sin(\beta-\varepsilon)}{\sin\alpha} & \dfrac{\sin(\gamma+\varepsilon)}{-\sin\alpha} \\ \dfrac{\cos(\beta-\varepsilon)}{-\sin\alpha} & \dfrac{\cos(\gamma+\varepsilon)}{-\sin\alpha} \end{bmatrix} \\ \boldsymbol{\mu}_2 = \begin{bmatrix} \dfrac{\sin(\beta-\varepsilon)\cos(\gamma+\varepsilon)}{-\sin\alpha} & \dfrac{\sin(\beta-\varepsilon)\sin(\gamma+\varepsilon)}{\sin\alpha} \\ \dfrac{\cos(\beta-\varepsilon)\cos(\gamma+\varepsilon)}{\sin\alpha} & \dfrac{\cos(\beta-\varepsilon)\sin(\gamma+\varepsilon)}{-\sin\alpha} \end{bmatrix} \\ \boldsymbol{\mu}_3 = \begin{bmatrix} \dfrac{\cos(\beta-\varepsilon)\sin(\gamma+\varepsilon)}{-\sin\alpha} & \dfrac{\sin(\beta-\varepsilon)\sin(\gamma+\varepsilon)}{-\sin\alpha} \\ \dfrac{\cos(\beta-\varepsilon)\sin(\gamma+\varepsilon)}{-\sin\alpha} & \dfrac{\sin(\beta-\varepsilon)\cos(\gamma+\varepsilon)}{-\sin\alpha} \end{bmatrix} \end{cases} \tag{12}$$

It is remarked that Δl_v is associated with the pose deviation of the first part. In the coordinate system O_1-$x_1y_1z_1$, the ideal virtual link is given by

$$\boldsymbol{l}_v = \boldsymbol{r} + \boldsymbol{l}_b \tag{13}$$

where $\boldsymbol{r} = [r_x, r_y, r_z]^T$ and $\boldsymbol{l}_{\mathrm{b}} = [-l_b, 0, 0]^T$ are the vector from O to A and the vector from A to B, respectively. Here, l_b is the length of AB. Considering the influence of the pose deviation of the first part, Eq. (13) is modified as

$$\boldsymbol{l}_v' = \boldsymbol{r} + \Delta \boldsymbol{r} + \Delta \boldsymbol{R} \cdot \boldsymbol{l}_b \tag{14}$$

in $\mathrm{O_g} - x_{\mathrm{g}}y_{\mathrm{g}}z_{\mathrm{g}}$. According to Eqs. (13) and (14), the length deviation of the virtual link Δl_{v} is expressed by

$$\Delta l_v = \sqrt{(r_x + \Delta x - l_b)^2 + \left(r_y + \Delta y - \delta_z l_b\right)^2 + \left(r_z + \Delta z + \delta_y l_b\right)^2} - \sqrt{(r_x - l_b)^2 + r_y^2 + r_z^2} \tag{15}$$

By substituting Eqs. (12) and (15) into Eq. (11), the position deviation of the point O can be calculated. Note that $\Delta \boldsymbol{O}$ is in the x_{g}-z_{g} plane, which only affect the orientation deviation around the y-axis. The deviation ξ_y is given by

$$\xi_y = \|\Delta \boldsymbol{O}\| / l_{02} \tag{16}$$

where $||\Delta \boldsymbol{O}||$ represents the norm of $\Delta \boldsymbol{O}$. Hence, we can obtain the assembly deviation δ of the ESS by integrating Eqs. (10) and (16) as follows:

$$\boldsymbol{\delta} = \Delta \boldsymbol{V} + \begin{bmatrix} 0 & 0 & 0 & 0 & \xi_y & 0 \end{bmatrix}^T \tag{17}$$

where $\boldsymbol{\delta} = [T_x; T_y; T_z; R_x; R_y; R_z]$. Specifically, the first three terms in $\boldsymbol{\delta}$ denotes the position deviation, while the last three terms describes the orientation deviation. Generally, the above assembly deviation model can be formulated as

$$\boldsymbol{\delta} = f(\boldsymbol{x}_d, \boldsymbol{p}) \tag{18}$$

where $\boldsymbol{x}_d \in \mathrm{R}^{7\times 1}$ is composed of the dimensional deviation of links, $\boldsymbol{p} \in \mathrm{R}^{21\times 1}$ is the vector that consists of the installation deviations of joints, and f represents the nonlinear mapping function.

In applications, the dimensional deviations of links are composed of the manufacturing deviations $\boldsymbol{x}_m \in \mathrm{R}^{7\times 1}$ and the adjustment vector $\boldsymbol{x} \in \mathrm{R}^{7\times 1}$, namely $\boldsymbol{x}_d = \boldsymbol{x} + \boldsymbol{x}_m$. Besides, there exists the initial shape deviation of the panels $\boldsymbol{\eta} \in \mathrm{R}^{6\times 1}$. Thus, Eq. (18) is further modified as

$$\boldsymbol{\delta} = f(\boldsymbol{x} + \boldsymbol{x}_m, \boldsymbol{p}) + \boldsymbol{\eta}. \tag{19}$$

According to Eq. (19), the assembly deviation of the ESS can be predicted, and the accuracy of this model will be verified in case studies.

III. SPARSE OPTIMIZATION FOR DIMENSIONAL ADJUSTMENT

A. PROBLEM FORMULATION OF DIMENSIONAL ADJUSTMENT

As studied in [29], [30], the assembly performance is evaluated by the weighted mean square of assembly deviation δ_w, which is defined as

$$\delta_w = \boldsymbol{\delta}^T \boldsymbol{Q} \boldsymbol{\delta} \tag{20}$$

where $\boldsymbol{Q} \in \mathrm{R}^{6\times 6}$ is a weighted coefficient matrix which represents the influence of different deviation items on the quality loss. The larger the coefficient related to the assembly deviation is, the more attention is paid to the accuracy index in assembly. After determining the objective function, we are considered with the assembly constraints. It is a fact that the assembly deviation control is conducted by manual operation, and the dimensional adjustment is of low efficiency. Moreover, the disassembly of links will cause damage to the reliability of key components such as springs and coating films, and the redundant adjustment may have influence on the deployed angles of self-locked joints. Therefore, the number of adjusted links is desired to be as few as possible under the same magnitude of deviation reduction. In this context, we aim to select n ($n \in \mathrm{R}^{\mathrm{N}+}$, $1 \le n \le 7$) links from all feasible ones, which means that n components of the decision vector $\boldsymbol{x}$ are nonzero. As discussed above, this optimization

problem is expressed as

$$\min_{\boldsymbol{x}} \ \delta_{\boldsymbol{w}} = [f(\boldsymbol{x}+\boldsymbol{x}_m, \boldsymbol{p}) + \boldsymbol{\eta}]^T \boldsymbol{Q} [f(\boldsymbol{x}+\boldsymbol{x}_m, \boldsymbol{p}) + \boldsymbol{\eta}]$$
$$\text{s.t. } \|\boldsymbol{x}\|_0 = n, \quad \boldsymbol{x}_l \le \boldsymbol{x} \le \boldsymbol{x}_u \tag{21}$$

where $\boldsymbol{x}_l$ and $\boldsymbol{x}_u$ are the lower and upper bounds of $\boldsymbol{x}$, respectively. $||\cdot||_0$ is the l_0 norm, which represents the number of nonzero components in $\boldsymbol{x}$.

Mathematically, the sparsity-constrained optimization can be intuitively transformed into a regularization problem [31]. However, the objective function including l_0 regularization is discontinuous, non-smooth and globally non-differentiable, and thus it is NP-hard to find the sparse solution of the optimization [32]. Previous research has proved that the solution of minimizing l_1 norm is also the sparsest solution for most underdetermined systems [33]. Hence, the optimization model as shown in Eq. (21) is transformed into a sparse optimization with l_1 norm:

$$\min_{\boldsymbol{x}} \ L(\boldsymbol{x}) = [f(\boldsymbol{x}+\boldsymbol{x}_m, \boldsymbol{p}) + \boldsymbol{\eta}]^T \boldsymbol{Q} [f(\boldsymbol{x}+\boldsymbol{x}_m, \boldsymbol{p}) + \boldsymbol{\eta}] + \lambda \|\boldsymbol{x}\|_1$$
$$\text{s.t. } \boldsymbol{x}_l \le \boldsymbol{x} \le \boldsymbol{x}_u \tag{22}$$

where the non-negative parameter λ is introduced to balance the assembly accuracy and the number of adjusted links. Obviously, the larger the value of λ is, the smaller the number of adjusted links will be. Thus, it can be inferred that there is at least a value of λ that satisfies the requirement of $||\boldsymbol{x}||_0 = n$ [34].

B. ALGORITHM FOR SPARSE OPTIMIZATION

Due to the existence of non-smooth term $||\boldsymbol{x}||_1$ and inequality constraints in the optimization problem (22), traditional convex optimization algorithms typically using gradient or sub-gradient techniques cannot be efficiently implemented [35]. In addition, the gradient method is very sensitive to the selection of the initial point and the step size, where improper parameters may lead to divergence. Recently, the ADMM [27], [36] has received much attention because of its broad applications in regularized estimation [37], resource allocation [38] and distributed learning [39]. The ADMM has several important theoretical properties as follows. First, the original constrained convex optimization problem is decomposed into multiple sub-problems whose solutions are coordinated to find the global optimum [27]. Second, the parameters of ADMM are updated with the superior convergence properties [37]. Besides, the ADMM has also been applied to solve nonconvex problems and the corresponding convergence analysis has been provided [40]. Hence, the ADMM is employed to solve the proposed optimization model in this study.

To convert (22) into a form appropriate for the ADMM, we first define an additional decision variable $\boldsymbol{z} \in \mathrm{R}^{7\times 1}$ by $\boldsymbol{x} = \boldsymbol{z}$. After this splitting of variables, the augmented Lagrangian function of problem (22) is given by

$$\min_{\boldsymbol{x}} \ L_\rho(\boldsymbol{x}, \boldsymbol{y}) = \boldsymbol{\delta}_{\boldsymbol{w}} + \omega + \lambda \|\boldsymbol{z}\|_1 + \boldsymbol{y}^T (\boldsymbol{x} - \boldsymbol{z}) + \frac{\rho}{2} \|\boldsymbol{x} - \boldsymbol{z}\|_2^2$$
$$\text{s.t. } \boldsymbol{x} - \boldsymbol{z} = 0 \tag{23}$$

where $\boldsymbol{y} \in \mathrm{R}^{7\times 1}$ is the dual variable, and ρ is the augmented Lagrangian parameter. Besides, ω is an indicator function of the constraint set $\mathrm{C} = \{\boldsymbol{x} \in \mathrm{R}^{7\times 1} : \boldsymbol{x}_l \le \boldsymbol{x} \le \boldsymbol{x}_u\}$, which is defined as:

$$\omega = \begin{cases} 0, & \boldsymbol{x} \in C \\ \infty, & \boldsymbol{x} \notin C \end{cases} \tag{24}$$

The ADMM generates a sequence of iterations by alternately minimizing the augmented Lagrangian function of the problem with respect to primal decision variable, and then updating the dual variable with the method of dual ascent. Let $h(\boldsymbol{x}) = \delta_w + \omega$, $k(\boldsymbol{z}) = \lambda||\boldsymbol{z}||_1$, and $\boldsymbol{u} = \boldsymbol{y}/\rho$. If we have the estimation $(\boldsymbol{x}^i, \boldsymbol{z}^i, \boldsymbol{u}^i)$ after i iterations, the parameters are updated by

$$\begin{cases} \boldsymbol{x}^{i+1} = \arg\min_{\boldsymbol{x}} \left(h(\boldsymbol{x}^i) + \frac{\rho}{2} \left\| \boldsymbol{x}^i - \boldsymbol{z}^i + \boldsymbol{u}^i \right\|_2^2 \right) \\ \boldsymbol{z}^{i+1} = \arg\min_{\boldsymbol{z}} \left(k(\boldsymbol{z}^i) + \frac{\rho}{2} \left\| \boldsymbol{x}^{i+1} - \boldsymbol{z}^i + \boldsymbol{u}^i \right\|_2^2 \right) \\ \boldsymbol{u}^{i+1} = \boldsymbol{u}^i + \boldsymbol{x}^{i+1} - \boldsymbol{z}^{i+1} \end{cases} \tag{25}$$

Given the formulas (25), the scaled form of the ADMM of the optimization problem can be derived as

$$\boldsymbol{x}^{i+1} = \arg\min_{\boldsymbol{x}} \left(h(\boldsymbol{x}^i) + (\boldsymbol{y}^i)^T \boldsymbol{x}^i + \frac{\rho}{2} \left\| \boldsymbol{x}^i - \boldsymbol{z}^i \right\|_2^2 \right), \tag{26}$$

$$\boldsymbol{z}^{i+1} = \text{Shrink}\left(\boldsymbol{x}^{i+1} + \left(\frac{1}{\rho} \right) \boldsymbol{y}^i, \frac{\lambda}{\rho} \right), \tag{27}$$

$$\boldsymbol{y}^{i+1} = \boldsymbol{y}^i + \rho \left(\boldsymbol{x}^{i+1} - \boldsymbol{z}^{i+1} \right). \tag{28}$$

Here, Shrink $(\boldsymbol{b}, c)$ is the shrinkage-thresholding operator, which is given by

$$\text{Shrink}(\boldsymbol{b}, c) = [H_c(b_1) \quad H_c(b_2) \quad \cdots \quad H_c(b_n)]^T. \tag{29}$$

In Eq. (29), $\boldsymbol{b} = [b_1, b_2, \ldots\ldots, b_n]^T$, and

$$H_c(b_n) = \text{sign}(b_n) \max\{|b_n| - c, 0\}. \tag{30}$$

According to the method of multipliers, the ADMM algorithm for the link adjustment is terminated when both the primal and dual residuals satisfy the following requirements:

$$\left\| \boldsymbol{x}^{i+1} - \boldsymbol{z}^{i+1} \right\|_2 < \varepsilon_p, \quad \left\| \boldsymbol{z}^{i+1} - \boldsymbol{z}^i \right\|_2 < \varepsilon_d \tag{31}$$

where $\varepsilon_p > 0$ and $\varepsilon_d > 0$ are feasibility tolerances. In this study, an absolute criterion and a relative criterion are employed to determine these tolerances, which are expressed as

$$\varepsilon_p = \sqrt{7} e_1 + e_2 \max\left\{ \left\| \boldsymbol{z}^i \right\|_2, \left\| \boldsymbol{x}^i \right\|_2 \right\}, \tag{32}$$

$$\varepsilon_d = \sqrt{7} e_1 + e_2 \rho \boldsymbol{u}^i, \tag{33}$$

where $e_1 > 0$ is the absolute tolerance and $e_2 > 0$ is the relative tolerance.

Let t be the maximum number of iterations, and the flowchart of the developed ADMM algorithm is shown in Figure 5. It is worth noting that the convergence of the ADMM is guaranteed according to [27], [31], [40], which

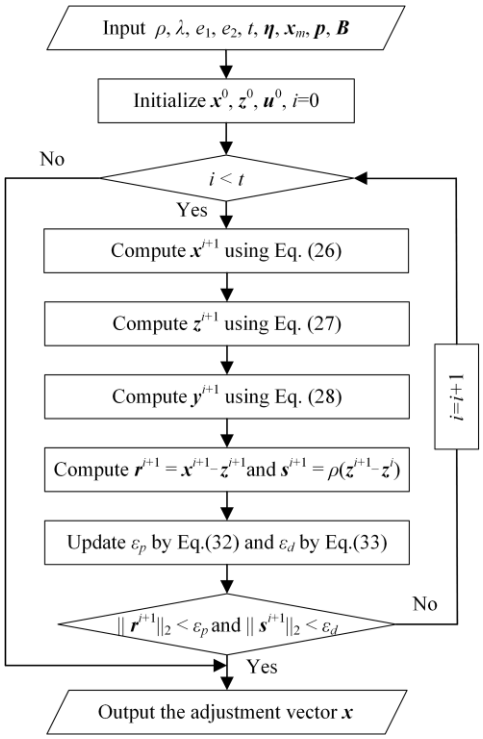

FIGURE 5. Flowchart of the proposed ADMM algorithm.

means that we can get the optimal combination of dimensional adjustments.

As mentioned above, the tuning parameter λ is introduced to control the sparsity of $\boldsymbol{x}$. On the one hand, decision-makers are allowed to freely set λ as a positive value if no strict limitations are imposed on the number of adjusted links. The larger λ is, the sparser the induced $\boldsymbol{x}$ will be. On the other hand, the value of λ that yields $||\boldsymbol{x}||_0 = n$ needs to be determined for the given number of adjusted links. In the latter case, a binary search algorithm is proposed to find a suitable value of λ.

To perform the binary search algorithm, the interval of λ needs to be first determined. Specifically, λ is located at the minimum value when all of the components in $\boldsymbol{x}$ are nonzero. That is, $\lambda_{\min} = 0$. On the contrary, the maximum value of λ will make all the components of $\boldsymbol{x}$ zero, which is derived as

$$\lambda_{\max} = 2 \left\| \boldsymbol{K}^T \boldsymbol{B} \left[f\left(\boldsymbol{x} + \boldsymbol{x}_m, \boldsymbol{p}\right) - \boldsymbol{K}\boldsymbol{x} + \boldsymbol{\eta} \right] \right\|_\infty \tag{34}$$

where $\boldsymbol{K}$ is the Jacobian matrix of the mapping function f with respect to $\boldsymbol{x}$, and $||\cdot||_\infty$ denotes the infinite norm. The proof of the maximum value is provided in appendix.

In summary, the whole binary search algorithm for estimating λ is shown in Figure 6.

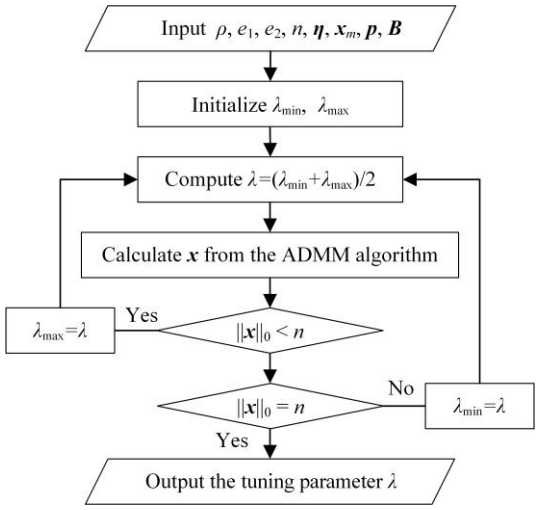

FIGURE 6. The binary search algorithm for estimating λ.

TABLE 1. Design dimensions of the ESS.

Structure parameters	Design dimensions /mm	Structure parameters	Design dimensions /mm
A_1A_2	1653.73	OA_1	2335.99
A_1A_3	2162.35	OA_3	883.80
A_3A_5	1802.87	OA_5	2007.84
OC	2147.51	AB	2221.24

IV. CASE STUDIES

A. VALIDATION OF THE ASSEMBLY DEVIATION MODEL

In above sections, we have derived the assembly deviation of the ESS in theory, and developed the sparse optimization model for dimensional adjustment of links as well as the corresponding solution strategy. In what follows, numerical case studies will be provided to demonstrate the implementation and validity of the proposed method.

As to the ESS for the space-borne SAR antenna, the design parameters are listed in Table 1. Each antenna panel is measured as 2220.00 mm (length) $\times$ 1650.00 mm (width) $\times$ 50.00 mm (height). The dimensional tolerance of the middle links is $\pm$ 0.26 mm, and that of other links is $\pm$ 0.44 mm. In addition, the installation deviations of joints are not more than 0.20 mm in the actual assembly process. The support links are made of the carbon fiber with the sectional area of 706.86 mm^2, and the antenna panels are composed of aluminum honeycombs [41]. The detailed Material properties of the ESS are shown in Table 2.

To validate the proposed methodology, the assembly deviation model is firstly compared with the FEA, which has been utilized to analyze the surface accuracy of other antennas [8], [10], [42]. According to the tolerances of current products, manufacturing and installation deviations are sampled to simulate the initial structural parameters, where 50 cases are generated with the method of Maximin Latin Hypercube Design [43]. In detail, the installation deviations of joints along z_g are modeled with sheets by Boolean operation in SOLODWORKS 2016, and other installation deviations are represented by the translation of connecting points. Considering that the extendible support structure works in space, the gravity of the structure can be ignored, and only the equivalent forces resulting from manufacturing deviations of links are applied in the endpoints of each link through the

TABLE 2. Material properties of the ESS.

Material properties	Value
Elastic modulus of links	550.00 Gpa
Poisson's ratio of links	0.30
Density of links	955.00 Kg/m3
Density of panels	1201.20 Kg/m3
Longitudinal elastic modulus of panels	334.90 Gpa
Transverse elastic modulus of panels	37.10 Gpa
Shear modulus G_{xy} / G_{xz} of panels	90.00 Mpa
Shear modulus G_{yz} of panels	63.00 Mpa

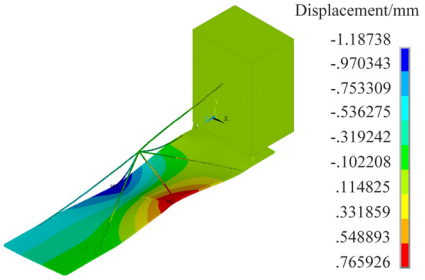

FIGURE 7. The finite element analysis of the assembly deviation.

temperature effect in ANSYS 2016. After the shape deformation shown in Figure 7 is obtained, the least square method is employed to construct the best-fitting plane, and the assembly deviation of the ESS is calculated by homogeneous coordinate transformation.

Figure 8 shows the root mean square error (RMSE) of predictions between the assembly deviation model and FEA, where the RMSE is defined by

$$\mathrm{RMSE} = \sqrt{\frac{1}{6}\left(\boldsymbol{\delta} - \boldsymbol{\delta}_f\right)^T \left(\boldsymbol{\delta} - \boldsymbol{\delta}_f\right)}. \tag{35}$$

Here, $\boldsymbol{\delta}_f \in \mathrm{R}^{6\times 1}$ denotes the assembly deviation obtained by FEA. In these 50 testing cases, the maximum and average of the RMSE are 0.7842×10^{-3} and 0.2622×10^{-3}, respectively. In order to further illustrate the performance of the model, the four cases with larger RMSE are presented in Table 3, and the corresponding results of the theoretical model and the FEA are listed in Table 4. For the position deviations, the absolute error between them is within 0.0013 mm; for the orientation deviations, it is less than 0.0007°. Therefore, the proposed assembly deviation model has good prediction accuracy.

B. ASSEMBLY DEVIATION CONTROL OF THE ESS

In practical engineering, it is required that R_y should be less than 0.02 °. It can be seen from Table 3 that the assembly accuracy of the ESS cannot be completely guaranteed in cases 1 and 4, even if manufacturing fluctuations and installation deviations meet the requirement of tolerances. In this section, $n = 3$ links are selected as an example from all those 7 possible links for assembly deviation control to validate the effectiveness of the proposed method. Considering R_y is associated with the pointing accuracy of SAR [13], the weight

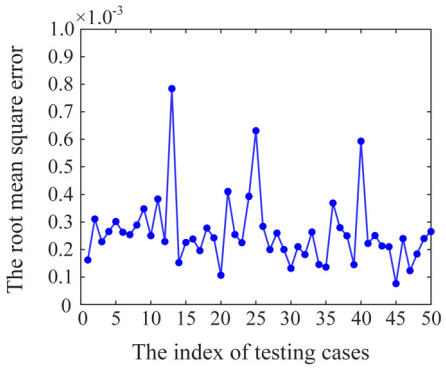

FIGURE 8. The root mean square error of the assembly deviation model.

TABLE 3. The manufacturing deviations of links and installation deviations of joints (Unit: mm).

Deviation sources		Case 1	Case 2	Case 3	Case 4
$\Delta \boldsymbol{l}$	Δl_1	0.13	-0.27	-0.18	-0.15
	Δl_2	-0.38	0.22	-0.06	0.28
	Δl_3	-0.13	0.19	0.11	-0.12
	Δl_4	0.19	-0.24	0.14	-0.18
	Δl_5	0.24	-0.46	-0.23	0.35
	Δl_6	0.25	-0.00	-0.18	-0.26
	Δl_0	-0.11	-0.36	0.17	0.42
$\Delta \boldsymbol{a}_1$	Δx_1	-0.05	0.05	0.13	-0.09
	Δy_1	-0.02	0.02	0.03	0.06
	Δz_1	-0.04	0.01	0.02	0.08
$\Delta \boldsymbol{a}_2$	Δx_2	-0.04	-0.03	0.17	0.10
	Δy_2	0.03	0.03	-0.08	-0.02
	Δz_2	0.02	-0.02	0.10	-0.17
$\Delta \boldsymbol{a}_3$	Δx_3	-0.02	0.11	0.13	-0.11
	Δy_3	0.04	0.02	0.05	0.05
	Δz_3	-0.05	0.04	0.02	0.04
$\Delta \boldsymbol{a}_4$	Δx_4	-0.06	0.05	-0.17	0.13
	Δy_4	-0.01	0.02	-0.18	0.06
	Δz_4	0.03	-0.04	0.01	0.20
$\Delta \boldsymbol{a}_5$	Δx_5	0.05	-0.04	0.11	-0.17
	Δy_5	-0.03	-0.02	0.17	-0.02
	Δz_5	-0.10	0.03	-0.15	-0.16
$\Delta \boldsymbol{a}_6$	Δx_6	-0.04	-0.02	0.03	0.08
	Δy_6	0.02	0.03	-0.01	-0.10
	Δz_6	0.03	-0.04	-0.20	0.11
$\Delta \boldsymbol{C}$	Δx_C	0.05	0.02	-0.04	-0.18
	Δz_C	-0.06	0.02	0.17	-0.03

of the assembly deviation is set to 2, and the other items are set to 1. Namely, $\boldsymbol{Q} = diag\ (1, 1, 1, 1, 2, 1)$. It should be pointed out that the weighted coefficient matrix $\boldsymbol{Q}$ is not unique and it can also be determined with the method of the analytic hierarchy process and expert scoring in applications. According to the current assembly process, the range of dimensional adjustment is $[-1, 1]$. Besides, the initial deviation of panels is given by $\boldsymbol{\eta} = [-0.0430, 0, 0.0754, 0.0008, 0.0035, -0.0001]^T$.

TABLE 4. Comparison of the assembly deviation model (ADM) and finite element analysis (FEA).

Assembly deviation	Case 1		Case 2	
	ADM	FEA	ADM	FEA
T_x/mm	0.0144	0.0157	-0.0248	-0.0236
T_y/mm	0.0000	0.0001	-0.0000	-0.0002
T_z/mm	0.0708	0.0695	-0.1221	-0.1229
R_x/°	0.0014	0.0012	-0.0067	-0.0066
R_y/°	0.0221	0.0216	0.0177	0.0182
R_z/°	-0.0003	-0.0004	0.0014	0.0013
Assembly deviation	Case 3		Case 4	
	ADM	FEA	ADM	FEA
T_x/mm	-0.0342	-0.0349	-0.0353	-0.0362
T_y/mm	-0.0000	0.0001	0.0000	0.0000
T_z/mm	-0.1683	0.1688	-0.1736	-0.1740
R_x/°	-0.0001	-0.0001	0.0074	0.0078
R_y/°	0.0180	0.0175	0.0278	0.0271
R_z/°	0.0000	-0.0001	-0.0015	-0.0014

TABLE 5. Result of link adjustment of links.

Adjustment	Case 1	Case 2	Case 3	Case 4
Δl_1/mm	–	0.46	–	–
Δl_2/mm	0.24	–	–	–
Δl_3/mm	–	-0.1	0.26	0.3
Δl_4/mm	-0.28	–	–	–
Δl_5/mm	–	-0.18	-0.04	-0.12
Δl_6/mm	-0.46	–	–	–
Δl_0/mm	–	–	-0.18	-0.38

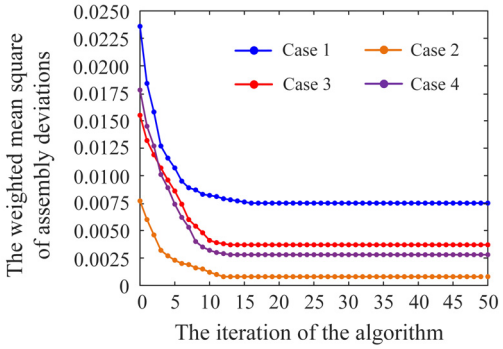

FIGURE 9. The weighted mean square of assembly deviations.

TABLE 6. Result of assembly performance under different number of adjusted links.

n	MPD/mm	MOD/°	RMSD
7	0.0228	0.0093	0.0012
6	0.0344	0.0117	0.0028
5	0.0383	0.0148	0.0041
4	0.0406	0.0172	0.0046
3	0.0481	0.0186	0.0075
2	0.0574	0.0197	0.0092
1	0.0692	0.0205	0.0128
0	0.1462	0.0256	0.0235

The algorithm parameters are set as $\rho = 2$, $e_1 = 10^{-4}$ and $e_2 = 10^{-2}$, which are regular settings of the ADMM. As shown in Figure 5, the algorithm is initialized with $\boldsymbol{x}^0 = -\boldsymbol{x}_m$, $\boldsymbol{z}^0 = \boldsymbol{0}$ and $\boldsymbol{u}^0 = \boldsymbol{0}$. Due to the quick convergence of ADMM, the maximum number of iterations t is set to 50. In our problem, the ADMM is performed in MATLAB R2015b and it only takes 37.2 s to find the optimal combination of link adjustments with Intel Core-i7-9750H CPU @2.60 GHz processor. Hence, the computational efficiency of the optimization algorithm is satisfying. Table 5 shows the strategy of link adjustment for above four cases, where "–" represents that there is no adjustment for the link.

It can be seen from Table 5 that the developed algorithm guarantees the sparsity of adjustment vector, and only three links are selected to be resized for reducing the assembly deviation of the ESS. Moreover, Table 5 also shows that different adjustment strategies are provided to deal with different manufacturing and installation deviations. Since the dimensional adjustment tends to select the most sensitive links to control the assembly deviation, these optimization results indicate that the sensitivity coefficient of each link is not constant, which is the reason why the fixed adjustment strategy adopted by current practice often fails to obtain the desired assembly accuracy.

To further validate the efficiency and effectiveness of the proposed method, Figure 9 presents the value of δ_w in the process of optimization, and it can be seen that the algorithm converges within 20 iterations. As a result, the optimized R_y of the ESS in these four cases are 0.0073°, 0.0061°, 0.0065° and 0.0018°, respectively. In comparison with the original orientation deviations (0.0256°, 0.0212°, 0.0215° and 0.0313°), the approach not only restores the unsatisfactory assembly accuracy to the desired assembly performance, but also significantly improves the assembly accuracy with an average increase of 79.56% in terms of the δ_w.

V. DISCUSSION

This paper develops an assembly deviation model and sparse optimization algorithm to obtain the strategy of link adjustment for the ESS, which are validated by the aforementioned numerical studies. It should be pointed out that the proposed method is not limited to achieve the optimal adjustment on the condition of fixed number of links, and it can also be used to determine the minimum number of links under the given requirement of assembly deviation control. For the reason that the proposed binary search algorithm is capable of providing a suitable λ such that $||\boldsymbol{x}||_0 = n$, we can choose the better adjustment strategy according to the optimization results of assembly deviations. Here, in addition to the root mean square of assembly deviations (RMSD), other two quantitative indexes are introduced to evaluate the assembly performance of ESS, which are the maximum position deviation (MPD) and the maximum orientation deviation (MOD).

Taking Case 1 as an example, we impose the constraint $n = 7, 6, 5, 4, 3, 2, 1$ on the proposed optimization method in sequence. After performing the binary search algorithm, the results of assembly performance under different number of adjusted links are listed in Table 6. Notably, the method tends to adjust more links to meet higher requirement of these

indexes, which is consistent with the domain experience. Given the engineering requirements of MPD $\leq$ 0.05 mm, MOD $\leq$ 0.02 ° and RMSD $\leq$ 0.005, $n = 4$ is the minimum number of adjusted links in this sample. If only the index MOD $\leq$ 0.02 ° is concerned, the assembly deviation control can be achieved by adjusting only 2 links, which is beneficial to improve the assembly efficiency and system reliability.

VI. CONCLUSION

In this study, we propose a novel method to optimize dimensional adjustment of links for the assembly deviation control of the ESS. First, the theoretical model is built to reveal the relationship between the assembly deviation and variation sources including manufacturing imperfections and installation deviations. Considering the characteristic of multiple closed-loops, the structural equivalent transformation is proposed to eliminate the abundant constraints, and the prediction performance of the proposed model is demonstrated with FEA. Afterward, the sparse optimization is developed to tackle the challenges of link adjustment. Aiming to select the optimal strategy for reducing assembly deviations, we establish the constrained optimization model of link adjustment in view of the assembly efficiency and system reliability, where it is preferred to adjust fewer links under the same magnitude of deviation reduction. Finally, the ADMM algorithm and the binary search are integrated to efficiently estimate the decision parameters, thereby acquiring the optimal combination of link adjustment.

Case studies illustrate the effectiveness of our methodology. The maximum and average values of the RMSE between the prediction results of the theoretical model and the FEA are 0.7842×10^{-3} and 0.2622×10^{-3}, respectively. This substantially indicates that the assembly deviation model is good enough to make predictions. Furthermore, the optimal strategy of link adjustment is obtained by minimizing the weighted mean square of assembly deviations. Specifically, the proposed method is able to not only achieve the optimal adjustment under the condition of fixed number of links, but also determine the minimum number of links given the requirement of assembly accuracy control.

In conclusion, the proposed approaches effectively overcome the limitations of current practice in the assembly of the ESS. Instead of trial and error, the precise strategy of link adjustment is provided to achieve the desired assembly accuracy, which significantly improves the product performance at a lower assembly cost.

APPENDIX

The maximum value of λ for the binary search means that all the components of vector $\boldsymbol{x}$ are penalized into zero. That is, we need to prove the proposition: if $\lambda \geq \lambda_{\max} = 2||\boldsymbol{K}^T\boldsymbol{B}\,[f\,(\boldsymbol{x}+\boldsymbol{x}_m,\boldsymbol{p}) - \boldsymbol{K}\boldsymbol{x}+\boldsymbol{\eta}]||_\infty$, $\boldsymbol{x} = \boldsymbol{0}$. According to the first-order condition of the optimization model (22), we have

$$2\boldsymbol{K}^T\boldsymbol{B}\,[f\,(\boldsymbol{x}+\boldsymbol{x}_m,\boldsymbol{p}) + \boldsymbol{\eta}] + \lambda\partial\,\|\boldsymbol{x}\|_1 = 0. \tag{A.1}$$

And then the equation is multiplied with $\boldsymbol{x}^T$, expressed as

$$2\boldsymbol{x}^T\boldsymbol{K}^T\boldsymbol{B}\,[\boldsymbol{K}\boldsymbol{x}+f\,(\boldsymbol{x}+\boldsymbol{x}_m,\boldsymbol{p}) - \boldsymbol{K}\boldsymbol{x}+\boldsymbol{\eta}] + \lambda\,\langle\boldsymbol{x},\,\partial\,\|\boldsymbol{x}\|_1\rangle = 0. \tag{A.2}$$

Since the weight matrix $\boldsymbol{B}$ is a positive diagonal matrix, $\boldsymbol{K}^T\boldsymbol{B}\boldsymbol{K}$ is symmetric positive definite. Hence, the following equation is satisfied:

$$\begin{aligned} 0 &\leq 2\boldsymbol{x}^T\boldsymbol{K}^T\boldsymbol{B}\boldsymbol{K}\boldsymbol{x} \\ &= -2\boldsymbol{x}^T\boldsymbol{K}^T\boldsymbol{B}\,[f\,(\boldsymbol{x}+\boldsymbol{x}_m,\boldsymbol{p}) - \boldsymbol{K}\boldsymbol{x} + \boldsymbol{\eta}] - \lambda\,\langle\boldsymbol{x},\,\partial\,\|\boldsymbol{x}\|_1\rangle\,. \end{aligned} \tag{A.3}$$

It is noted that

$$\partial\,\|\boldsymbol{x}_i\|_1 = \begin{cases} 1, & \boldsymbol{x}_i > 0 \\ -1, & \boldsymbol{x}_i < 0 \\ [-1,\,1], & \boldsymbol{x}_i = 0. \end{cases} \tag{A.4}$$

If $\lambda \geq 2||\boldsymbol{K}^T\boldsymbol{B}\,[f\,(x_d,\boldsymbol{p}) - \boldsymbol{K}\boldsymbol{x} + \varepsilon]||_\infty$, we can obtain

$$\begin{aligned} &\operatorname{sign}\left(2\boldsymbol{K}^T\boldsymbol{B}\,[f\,(\boldsymbol{x}+\boldsymbol{x}_m,\boldsymbol{p}) + \boldsymbol{\eta}] - \boldsymbol{K}\boldsymbol{x} + \lambda\partial\,\|\boldsymbol{x}\|_1\right)_i \\ &\qquad = \operatorname{sign}(\boldsymbol{x}_i) \quad (i \in S = \{i : \boldsymbol{x}_i \neq 0\}) \end{aligned} \tag{A.5}$$

where $\operatorname{sign}(x) = -1$ for $x \leq 0$ and 1 otherwise. However, it can be derived that

$$\begin{aligned} &2\boldsymbol{x}^T\boldsymbol{K}^T\boldsymbol{B}\,[f\,(\boldsymbol{x}+\boldsymbol{x}_m,\boldsymbol{p}) - \boldsymbol{K}\boldsymbol{x} + \boldsymbol{\eta}] + \lambda\,\langle\boldsymbol{x},\,\partial\,\|\boldsymbol{x}\|_1\rangle \\ &= \left(\boldsymbol{x}^T\right)_S\left(2\boldsymbol{K}^T\boldsymbol{B}\,[f\,(\boldsymbol{x}+\boldsymbol{x}_m,\boldsymbol{p}) - \boldsymbol{K}\boldsymbol{x} + \boldsymbol{\eta}] + \lambda\partial\,\|\boldsymbol{x}\|_1\right)_S \\ &\quad + \left(\boldsymbol{x}^T\right)_{S^c}\left(2\boldsymbol{K}^T\boldsymbol{B}\,[f\,(\boldsymbol{x}+\boldsymbol{x}_m,\boldsymbol{p}) - \boldsymbol{K}\boldsymbol{x} + \boldsymbol{\eta}] + \lambda\partial\,\|\boldsymbol{x}\|_1\right)_{S^c} \\ &= \left(\boldsymbol{x}^T\right)_S\left(2\boldsymbol{K}^T\boldsymbol{B}\,[f\,(\boldsymbol{x}+\boldsymbol{x}_m,\boldsymbol{p}) - \boldsymbol{K}\boldsymbol{x} + \boldsymbol{\eta}] + \lambda\partial\,\|\boldsymbol{x}\|_1\right)_S \\ &> 0 \end{aligned} \tag{A.6}$$

where S^C represents the complementary set of S, and Eq. (A.6) is obviously contradictory with Eq. (A.3). Thus, there is no nonzero components in vector $\boldsymbol{x}$ if $\lambda \geq \lambda_{\max} = 2||\boldsymbol{K}^T\boldsymbol{B}\,[f\,(\boldsymbol{x}+\boldsymbol{x}_m,\boldsymbol{p}) - \boldsymbol{K}\boldsymbol{x} + \boldsymbol{\eta}]||_\infty$, and the proof is completed.

ACKNOWLEDGMENT

The authors appreciate the valuable discussion with Feifei Chen, who is an Engineer of the Institute of Aerospace Systems Engineering in Shanghai.

REFERENCES

[1] Z. Wu, L. Zhang, and H. Liu, "Generalized three-dimensional imaging algorithms for synthetic aperture radar with metamaterial apertures-based antenna," *IEEE Access*, vol. 7, pp. 59716–59727, Apr. 2019.

[2] X. Ye, F. Zhang, Y. Yang, D. Zhu, and S. Pan, "Photonics-based high-resolution 3D inverse synthetic aperture radar imaging," *IEEE Access*, vol. 7, pp. 79503–79509, Jun. 2019.

[3] A. Reigber, R. Scheiber, M. Jager, P. Prats-Iraola, I. Hajnsek, T. Jagdhuber, K. P. Papathanassiou, M. Nannini, E. Aguilera, S. Baumgartner, R. Horn, A. Nottensteiner, and A. Moreira, "Very-high-resolution airborne synthetic aperture radar imaging: Signal processing and applications," *Proc. IEEE*, vol. 101, no. 3, pp. 759–783, Mar. 2013.

[4] W. D. R. Thomas, "RADARSAT-2 extendible support structure," *Can. J. Remote Sens.*, vol. 30, no. 3, pp. 282–286, Jun. 2004.

[5] Q. Zhao, J. Guo, J. Hong, and Z. Liu, "Analysis of angular errors of the planar multi-closed-loop deployable mechanism with link deviations and revolute joint clearances," *Aerosp. Sci. Technol.*, vol. 87, pp. 25–36, Apr. 2019.

[6] Y. Yang, S. Xie, W. Zhang, J. Luo, and H. Li, "Accuracy model, analysis, and adjustment in the context of multi-closed-loop planar deployable mechanisms," *Adv. Mech. Eng*, vol. 8, no. 3, pp. 1–15 Mar. 2016.
[7] Q. Zhao, J. Guo, D. Yu, J. Hong, and F. Chen, "An enhanced method of resizing support links for a planar closed-loop overconstrained deployable structure considering kinematic reliability and surface accuracy," *Aerosp. Sci. Technol.*, vol. 104, Sep. 2020, Art. no. 105988, doi: 10.1016/j.ast.2020.105988.
[8] M. Mobrem, "Methods of analyzing surface accuracy of large antenna structures due to manufacturing tolerances," in *Proc. 44th AIAA/ASME/ASCE/AHS/ASC Struct., Structural Dyn., Mater. Conf.*, no. 1453, Apr. 2003, pp. 1–10.
[9] J. Du, C. Wang, H. Bao, and L. Wang, "Robust shape adjustment with finite element model updating for mesh reflectors," *AIAA J.*, vol. 55, no. 4, pp. 1–10, Jan. 2017.
[10] F. Zheng, J. He, and P. Zhang, "Simulating evaluation of new space deployable antenna," *Aircr. Eng. Aerosp. Technol.*, vol. 88, no. 6, pp. 835–845, Oct. 2016.
[11] J. Wu, C. Wang, and H. Wang, "Accuracy analysis of satellite antenna plate deployment based on Monte Carlo method," *Spacecraft Recovery Remote Sens.*, vol. 34, no. 6, pp. 89–94, Dec. 2013.
[12] Y. Yang, J. Luo, W. Zhang, S. Xie, Y. Sun, and H. Li, "Accuracy analysis of a multi-closed-loop deployable mechanism," *Proc. Inst. Mech. Eng. C, J. Mech. Eng. Sci.*, vol. 230, no. 4, pp. 611–621, Mar. 2016.
[13] X. Li, X. Ding, and G. S. Chirikjian, "Analysis of angular-error uncertainty in planar multiple-loop structures with joint clearances," *Mechanism Mach. Theory*, vol. 91, pp. 69–85, Sep. 2015.
[14] Q. Zhao, J. Guo, and J. Hong, "Assembly precision prediction for planar closed-loop mechanism in view of joint clearance and redundant constraint," *J. Mech. Sci. Technol.*, vol. 32, no. 7, pp. 3395–3405, Jul. 2018.
[15] K.-L. Ting and Y.-W. Liu, "Rotatability laws for N-bar kinematic chains and their proof," *J. Mech. Des.*, vol. 113, no. 1, pp. 32–39, Mar. 1991.
[16] T.-H. Lee, R. C. Ruddock, and M. C. Bailey, "A surface distortion analysis applied to the hoop/column deployable mesh reflector antenna," *IEEE Trans. Antennas Propag.*, vol. 37, no. 4, pp. 452–458, Apr. 1989.
[17] R. Liu, H. Guo, R. Liu, H. Wang, D. Tang, and X. Song, "Shape accuracy optimization for cable-rib tension deployable antenna structure with tensioned cables," *Acta Astronautica*, vol. 140, pp. 66–77, Nov. 2017.
[18] T. Li, H. Deng, and Y. Tang, "Mathematical relationship between mean cable tensions and structural parameters of deployable reflectors," *Aerosp. Sci. Technol.*, vol. 56, pp. 205–211, Sep. 2016.
[19] Y. Tang, T. Li, Z. Wang, and H. Deng, "Surface accuracy analysis of large deployable antennas," *Acta Astron.*, vol. 104, no. 1, pp. 125–133, Nov. 2014.
[20] P. D. Maddio, A. Meschini, R. Sinatra, and A. Cammarata, "An optimized form-finding method of an asymmetric large deployable reflector," *Eng. Struct.*, vol. 181, pp. 27–34, Feb. 2019.
[21] Z. Chu, Z. Deng, X. Qi, and B. Li, "A task-space form-finding algorithm for tensegrity robots," *Acta Astronaut.*, vol. 95, pp. 51–60, Mar. 2014.
[22] X. Li, W. Kong, and J. He, "Form-finding of deployable mesh reflectors using dynamic relaxation method," *IEEE Access*, vol. 8, pp. 100578–100585, May 2020.
[23] S. Zhang, J. Du, D. Yang, Y. Zhang, and S. Li, "A combined shape control procedure of cable mesh reflector antennas with optimality criterion and integrated structural electromagnetic concept," *Struct. Multidisciplinary Optim.*, vol. 55, no. 1, pp. 289–295, Jan. 2017.
[24] T. Li, Y. Tang, and T. Zhang, "Surface adjustment method for cable net structures considering measurement uncertainties," *Aerosp. Sci. Technol.*, vol. 59, pp. 52–56, Dec. 2016.
[25] J. Du, Y. Gu, H. Bao, C. Wang, and X. Chen, "Shape adjustment optimization and experiment of cable-membrane reflectors," *Acta Astron.*, vol. 146, pp. 192–201, May 2018.
[26] C. Liu and Y. Shi, "Comprehensive structural analysis and optimization of the electrostatic forming membrane reflector deployable antenna," *Aerosp. Sci. Technol.*, vol. 53, pp. 267–279, Jun. 2016.
[27] S. Boyd, N. Parikh, and E. Chu, "Distributed optimization and statistical learning via the alternating direction method of multipliers," *Mach. Learn.*, vol. 3, no. 1, pp. 1–122, Jun. 2010.
[28] R. P. Paul, *Robot Manipulators: Mathematics, Programming, and Control: The Computer Control of Robot Manipulators*, 1st ed. Boston, MA, USA: MIT Press, 1981, pp. 82–90.
[29] Y. He, F. Wang, Y. Li, J. Qin, and B. Chen, "Robust matrix completion via maximum correntropy criterion and half-quadratic optimization," *IEEE Trans. Signal Process.*, vol. 68, pp. 181–195, Nov. 2020.
[30] M. V. Minniti, F. Farshidian, R. Grandia, and M. Hutter, "Whole-body MPC for a dynamically stable mobile manipulator," *IEEE Robot. Autom. Lett.*, vol. 4, no. 4, pp. 3687–3694, Oct. 2019.
[31] C. Duan, W. Fang, L. Jiang, and S. Niu, "FACTS devices allocation via sparse optimization," *IEEE Trans. Power Syst.*, vol. 31, no. 2, pp. 1308–1319, Mar. 2016.
[32] B. K. Natarajan, "Sparse approximate solutions to linear systems," *SIAM J. Comput.*, vol. 24, no. 2, pp. 227–234, Apr. 1995.
[33] D. L. Donoho, "For most large underdetermined systems of linear equations the minimal ℓ_1-norm solution is also the sparsest solution," *Commun. Pure Appl. Math.*, vol. 59, no. 6, pp. 797–829, Jun. 2006.
[34] J. Du, X. Yue, J. H. Hunt, and J. Shi, "Optimal placement of actuators via sparse learning for composite fuselage shape control," *J. Manuf. Sci. Eng.*, vol. 141, no. 10, pp. 1–12, Oct. 2019.
[35] S. Boyd and L. Vandenberghe, *Convex Optimization*. Cambridge, U.K.: Cambridge Univ. Press, 2004.
[36] Q. Liu, X. Shen, and Y. Gu, "Linearized ADMM for nonconvex nonsmooth optimization with convergence analysis," *IEEE Access*, vol. 7, pp. 76131–76144, May 2019.
[37] J. Liang, X. Zhang, H. C. So, and D. Zhou, "Sparse array beampattern synthesis via alternating direction method of multipliers," *IEEE Trans. Antennas Propag.*, vol. 66, no. 5, pp. 2333–2345, May 2018.
[38] L. Jian, J. Hu, J. Wang, and K. Shi, "Distributed inexact dual consensus ADMM for network resource allocation," *Optim. Control Appl. Methods*, vol. 40, no. 6, pp. 1071–1087, Nov. 2019.
[39] A. Elgabli, J. Park, A. S. Bedi, C. B. Issaid, M. Bennis, and V. Aggarwal, "Q-GADMM: Quantized group ADMM for communication efficient decentralized machine learning," *IEEE Trans. Commun.*, vol. 69, no. 1, pp. 164–181, Jan. 2021, doi: 10.1109/TCOMM.2020.3026398.
[40] Y. Wang, W. Yin, and J. Zeng, "Global convergence of ADMM in nonconvex nonsmooth optimization," *J. Sci. Comput.*, vol. 78, no. 1, pp. 29–63, Jan. 2019.
[41] P. R. Akbar, H. Saito, M. Zhang, J. Hirokawa, and M. Ando, "Parallel-plate slot array antenna for deployable SAR antenna onboard small satellite," *IEEE Trans. Antennas Propag.*, vol. 64, no. 5, pp. 1661–1671, May 2016.
[42] X. Li and J.-M. Jin, "A comparative study of three finite element-based explicit numerical schemes for solving Maxwell's equations," *IEEE Trans. Antennas Propag.*, vol. 60, no. 3, pp. 1450–1457, Mar. 2012.
[43] K. Le Guiban, A. Rimmel, M.-A. Weisser, and J. Tomasik, "The first approximation algorithm for the maximin Latin hypercube design problem," *Oper. Res.*, vol. 66, no. 1, pp. 253–266, Feb. 2018.